

ARTICLE

Scintillation Level of Scattered Radio Waves in the Equatorial Ionosphere

George Jandieri^{1*}, Zaza Sanikidze², Nino Mchedlishvili³

¹ Department of Stochastic Analysis and Mathematical Simulation, International Space Agency Georgian Society, Georgian Technical University, Tbilisi, 0175, Georgia

² Muskhelishvili Institute of Computational Mathematics, Georgian Technical University, Tbilisi, 0175, Georgia

³ Department of Control System, Georgian Technical University, Tbilisi, 0175, Georgia

ABSTRACT

Scintillation effects of propagating and scattered radio waves (RWs) are considered analytically and numerically in the equatorial terrestrial ionosphere applying the statistical characteristics. Analytical calculations of the second-order statistical moments of the phase fluctuations of the ordinary and extraordinary RWs in the conductive collision ionospheric magnetoplasma (COCOIMA) are carried out for the first time using the Wentzel-Kramers-Brillouin method and the modified smooth perturbation method in consideration of the diffraction effects. Polarization coefficients of these waves in the equatorial ionosphere have been derived for the first time. The scintillation level includes the variance and the correlation functions of scattered RWs. Statistical moments contain complex refractive index, anisotropy coefficient characterizing irregular plasmonic structures, tilt angle of prolate irregularities concerning to the external magnetic field, permittivity components of the equatorial ionosphere, Hall's, Pedersen and longitudinal conductivities. A new feature of the "Fountain Effect" has been discovered in the equatorial ionosphere at weak and moderate scintillations caused due to anisotropy parameters of electron density fluctuations. Anisotropy parameters of electron density inhomogeneities influence the scintillation index of both the ordinary and extraordinary radio waves shifting maximums of the curves in the opposite directions at weak and moderate scintillations. Numerical calculations are carried out using the hybrid anisotropic correlation function of electron density fluctuations containing both exponential and power-law spectral functions having arbitrary spectral index, applying the experimental data.

Keywords: Radio waves; Statistical characteristics; Atmosphere; Conductivity; Scintillation; Irregularities; Ordinary and extraordinary waves

*CORRESPONDING AUTHOR:

George Jandieri, Department of Stochastic Analysis and Mathematical Simulation, International Space Agency Georgian Society, Georgian Technical University, Tbilisi, 0175, Georgia; Email: georgejandieri7@gmail.com

ARTICLE INFO

Received: 17 May 2024 | Revised: 24 May 2024 | Accepted: 27 May 2024 | Published Online: 25 June 2024

DOI: <https://doi.org/10.30564/jees.v6i2.6643>

CITATION

Jandieri, G., Sanikidze, Z., Mchedlishvili, N., 2024. Scintillation Level of Scattered Radio Waves in the Equatorial Ionosphere. Journal of Environmental & Earth Sciences. 6(2): 99–109. DOI: <https://doi.org/10.30564/jees.v6i2.6643>

COPYRIGHT

Copyright © 2024 by the author(s). Published by Bilingual Publishing Group. This is an open access article under the Creative Commons Attribution-NonCommercial 4.0 International (CC BY-NC 4.0) License (<https://creativecommons.org/licenses/by-nc/4.0/>).

1. Introduction

Statistical moments of scattered RWs in a randomly inhomogeneous media are well studied^[1,2]. Transient size of ionospheric electron density inhomogeneities or total electron content (TEC) varies from a few meters to several tens of kilometers^[3,4]. Evolution of prolate electron density inhomogeneities is studied with a spatial fluctuation of TEC (SFT) maps containing the magnitude, shape, direction and intensity distribution of these inhomogeneities at lower latitudes. The set of anisotropic inhomogeneities is mainly directed in the north-south direction. The geomagnetic field leads to the birefringence of RWs generating both the ordinary (O-) and extraordinary (E-) waves. The error of the phase of the radio signal emitted by satellite radio navigation systems consists of the variance of the phase fluctuation of the radio signal, the variance of thermal noise and the variance of the generator's noise. Anisotropic electron density irregularities and spatial-temporal random variation of electron concentration in the ionosphere cause random variations of the amplitude and phase of the Global Positioning System (GPS) signals propagating via the ionosphere leading appropriately to the scintillation^[5,6]. Ionospheric scintillation leads to the enhancements and fading of the radio signals propagating in the night-time F-region at equatorial latitudes. Calculation of the statistical moments of RWs propagating in the equatorial terrestrial ionosphere and investigation of scintillation phenomena will have wide application in the Global Navigation Satellite System (GNSS).

Scintillation phenomena of RWs propagating in the high-latitude ionosphere were investigated in the studies of Jandieri et al.^[7-9]. Calculation of the statistical moments of scattered RWs in the equatorial ionosphere was considered in the studies of Jandieri.^[10,11] The morphology of scintillations was described by second order statistical moments of scattered RWs.

Ionospheric irregularities and scintillations of radio signals near the geomagnetic equator were observed^[12] by three identical Swarm satellites. These studies are based on the weak scintillation theory. Equatorial phase scintillations have been used to get

information about the power spectrum of electron density inhomogeneities, which leads to the scintillations, as well as the inhomogeneities drift velocities transverse to the signal path. Characteristic linear scale of the inhomogeneities leading to the scintillation can be defined directly from the baseline dependence of the scintillation index.

Radar backscatter and AE-C satellites observations show that in low-latitude ionosphere near the equator after midnight electron density inhomogeneities in the topside ionosphere are field-aligned plasma density depletion structures with dimensions from a few meters to several tens of kilometers^[13,14]. Statistical characteristics of the phase fluctuations and the equatorial scintillation phenomena based on rocket (bottomside) and satellite (topside) measurements of plasmonic inhomogeneities (for example “plume-like” and wedge).

It was established that the nonlinear Rayleigh-Taylor instability (RTI) on the bottom side of the F-peak generates upwelling plume structures and large-scale equatorial plasma bubbles (EPBs)^[15-21] during the nighttime, post-sunset hours; then they rise, develop and propagate on a high-latitudes along the geomagnetic lines of forces. EPBs may travel across different longitudes changing their shape and strength of inhomogeneities. They are classified as large (> 100 km), intermediate (10 km–100 m), and small (< 100 m) scale structures, respectively^[19].

For a sufficiently thin layer of inhomogeneities, amplitude random variations inside the layer are very small and phase variation on the incident radio wave is important. Application of the Wentzel-Kramers-Brillouin method to the equatorial bubble is used in obtaining the amplitude and phase variations on the ground. This theory allows us to investigate statistical peculiarities of electron density irregularities such as root-mean square deviations (RSD) of electron density and power spectra of the irregularities.

In section 2, the signal statistics—calculation of the RSD of the phase fluctuations are considered using the stochastic differential equation of the phase fluctuation taking into consideration diffraction effects. Polarization coefficients of the O- and E-

waves are calculated for the equatorial terrestrial ionosphere for the first time. Statistical characteristics are derived from the arbitrary correlation function of electron density fluctuations. In section 3, numerical calculations are carried out for the “hybrid” mutual coherence function (MCF) of the phase of a radio signal enrolled on the ground, using experimental data. The scintillation level is analyzed for different anisotropy coefficients and the inclination angle of prolate electron density irregularities for the geomagnetic lines of forces. Conclusions are made in section 4.

2. Materials and methods

In this section, second order statistical moments of scattered radio waves in the equatorial ionosphere are considered.

Wave equation for the electrical field (equation (1)):

$$(\nabla_i \nabla_j - \Delta \delta_{ij} - k_0^2 \tilde{\epsilon}_{ij}) E_j(\mathbf{r}) = 0 \quad (1)$$

where: $k_0 = \omega/c$ is the wavenumber of an incident wave having frequency ω ; Δ is the Laplacian, δ_{ij} is the Kronecker symbol, $\tilde{\epsilon}_{ij} = \epsilon_{ij} - i \tilde{\sigma}_{ij}$, $\tilde{\sigma}_{ij} \equiv \sigma_{ij} (4\pi/k_0 c)$ are the second rank permittivity and conductivity tensors of the COCOIMA plasma, respectively. Wave field offer as $E(\mathbf{r}) = E_0 \exp\{\Phi(\mathbf{r})\}$, where $\Phi(\mathbf{r})$ is the complex phase of the RW $\Phi(\mathbf{r}) = \varphi_0 + \varphi_1 + \varphi_2 + \dots$. First term $\varphi_0 = ik_0 z + ik_{\perp} y$, corresponds to an incident wave, in consideration of the diffraction effects, $k_{\perp} \ll k_0$; other terms are random functions of the spatial coordinates.

The normalized conductivity tensor $\tilde{\sigma} = 4\pi \hat{\sigma} / k_0 c$ of ionospheric plasma at equatorial latitude^[22] contains the Hall's σ_H , Pedersen σ_{\perp} and longitudinal σ_{\parallel} conductivities:

$$\sigma_H = e^2 n_e \left(\frac{\omega_e}{m_e (\nu_e^2 + \omega_e^2)} - \frac{\omega_i}{m_i (\nu_{in}^2 + \omega_i^2)} \right),$$

$$\sigma_{\perp} = e^2 n_e \left(\frac{\nu_e}{m_e (\nu_e^2 + \omega_e^2)} + \frac{\nu_i}{m_i (\nu_{in}^2 + \omega_i^2)} \right)$$

$$\sigma_{\parallel} = e^2 n_e \left(\frac{1}{m_e \nu_e} + \frac{1}{m_i \nu_{in}} \right),$$

e and m_e are the charge and mass of an electron, $\nu_e = \nu_{en} + \nu_{in}$ is the effective collision frequency of electrons with other plasma particles; ω_e and ω_i are the angular gyrofrequencies of an electron and ion, respectively; electron density $n_e(\mathbf{r})$ is a fluctuating term, $\nu_e = \nu_{en} + \nu_{in}$ is the effective collision frequency of electrons with ions and neutral particles

$$\nu_{ei} = N \left[59 + 4.18 \log \left(\frac{T_e^3}{N} \right) \right] \times 10^{-6} T_e^{-3/2} \quad [\text{m.k.s}]$$

and $\nu_{en} = 5.4 \times 10^{-16} N_n T_e^{1/2} \quad [\text{m.k.s}]$.

From equation (1) we obtain equation (2):

$$\begin{aligned} \frac{\partial \psi}{\partial x} + \frac{i}{k_x (E_{0z} / E_{0x}) - 2k_0} \left[k_x (k_y + k_{\perp}) (E_{0y} / E_{0x}) \right. \\ \left. + k_x k_0 (E_{0z} / E_{0x}) - k_y (k_y + 2k_{\perp}) \right] \psi \\ = -i \frac{k_0^2}{k_x (E_{0z} / E_{0x}) - 2k_0} \left(\tilde{\epsilon}_{xx}^{(1)} - i \tilde{\epsilon}_{xz}^{(1)} \frac{E_{0z}}{E_{0x}} \right) \end{aligned} \quad (2)$$

Here ψ is the Fourier transformation of the phase fluctuations.

Components of the dielectric permittivity for the equatorial ionosphere can be written as equation (3):

$$\begin{aligned} \tilde{\epsilon}_{xx} &= \epsilon_{\perp} - i \tilde{\sigma}_{\perp}, \quad \tilde{\epsilon}_{xy} = i (\mathfrak{a} + \tilde{\sigma}_H) \sin \theta, \\ \tilde{\epsilon}_{xz} &= i (\mathfrak{a} + \tilde{\sigma}_H) \cos \theta, \quad \tilde{\epsilon}_{yx} = -\tilde{\epsilon}_{xy}, \quad \tilde{\epsilon}_{zx} = -\tilde{\epsilon}_{xz}, \\ \tilde{\epsilon}_{yy} &= (\epsilon_{\perp} + p_0 u \cos^2 \theta) - i (\tilde{\sigma}_{\parallel} \cos^2 \theta + \tilde{\sigma}_{\perp} \sin^2 \theta), \\ \tilde{\epsilon}_{yz} &= -[p_0 u + i (\tilde{\sigma}_{\perp} - \tilde{\sigma}_{\parallel})] \sin \theta \cos \theta, \quad \tilde{\epsilon}_{zy} = \tilde{\epsilon}_{yz}, \\ \tilde{\epsilon}_{zz} &= (\epsilon_{\perp} + p_0 u \sin^2 \theta) - i (\tilde{\sigma}_{\parallel} \sin^2 \theta + \tilde{\sigma}_{\perp} \cos^2 \theta) \end{aligned} \quad (3)$$

where: $\epsilon_{\perp} = 1 - p_0$, $p_0 = v / (1 - u)$, $u = (eH_0 / m_e c \omega)^2$ are non-dimensional magneto-ionic parameters of the COCOIMA plasma, $\omega_p(\mathbf{r}) = [4\pi n_e(\mathbf{r}) e^2 / m_e]^{1/2}$ is the plasma frequency. They contain both regular and fluctuating terms (n_1).

Let a homogeneous external magnetic field lie in the YOZ plane and the wave vector $\mathbf{\kappa}$ is directed along the Y axis, θ is an angle between these vectors.

Complex refractive index of the COCOIMA plasma in the conductive equatorial ionosphere can be written as $N^2 = \Gamma_0 + i\Gamma_1$ [10], polarization coefficients of scattered RWs at $s \ll \varepsilon_{ij}$, $\tilde{\sigma}_{ij}$ can be written as equation (4):

$$P_{1,2} = \frac{\langle E_y \rangle}{\langle E_x \rangle} = P' - iP'' \quad , \quad G_{1,2} = \frac{\langle E_z \rangle}{\langle E_x \rangle} = -(G' + iG'') \quad (4)$$

The right part contains electron density fluctuations; the angular brackets denote an ensemble average, indices 1 and 2 are devoted to the O- and E-waves, respectively. Below indices in the polarization coefficients are omitted for brevity.

Taking into account the geometry of the task, the polarization coefficients obtain equations (5) and (6):

$$P_{1,2} = \frac{(\Psi_1\Psi_3 - \Psi_2\Psi_4) - i(\Psi_2\Psi_3 + \Psi_1\Psi_4)}{\Psi_3^2 + \Psi_4^2} \sin\theta = P' - iP'' \quad (5)$$

where: $\Psi_1 = (\sigma_{\parallel} - \sigma_{\perp})(\Gamma_1 + \sigma_{\perp}) + p_0u(\Gamma_0 - \varepsilon_{\perp}) - (\varkappa + \sigma_H)^2$, $\Psi_4 = \varepsilon_{\parallel}(\varkappa + \sigma_H)$, $\Psi_2 = (\sigma_{\parallel} - \sigma_{\perp})(\Gamma_0 + \Gamma_1 - \varepsilon_{\perp} + \sigma_{\perp})$, $\Psi_3 = (\varkappa + \sigma_H)[(\sigma_{\parallel} - \sigma_{\perp})\sin^2\theta + p_0u\cos^2\theta + \varepsilon_{\perp}]$.

$$G_{1,2} = -\frac{1}{F_1^2 + F_2^2} [(F_1F_3 + F_2F_4) + i(F_1F_4 - F_2F_3)] = -(G' + iG'') \quad (6)$$

where: $F_1 = \Gamma_0 - (\varepsilon_{\perp} + p_0u \sin^2\theta)$, $F_2 = \Gamma_1 + (\sigma_{\parallel} \sin^2\theta + \sigma_{\perp} \cos^2\theta)$, $F_3 = p_0uP' - (\sigma_{\parallel} - \sigma_{\perp})P''$, $F_4 = (\varkappa + \sigma_H)\cos\theta - P''p_0u - P'(\sigma_{\parallel} - \sigma_{\perp})$.

As a result, from equation (1) we obtain the stochastic differential equation (7)

$$\frac{\partial\psi}{\partial x} + \frac{k_0}{4}(C_0 + iC_1)\psi = \frac{k_0}{4}(e_0 + ie_1)n_1 \quad (7)$$

where: $C_0 = a_1b_0 - a_0b_1$, $C_1 = a_0b_0 + a_1b_1$, $a_0 = 2 + G'x$, $a_1 = G''x$, $b_0 = [G' - P'(y + \mu)]x + (y^2 + 2\mu y)$, $b_1 = [G'' + P''(y + \mu)]x$, $\mu = k_{\perp}/k_0$ is the diffraction parameter, $e_0 = a_1d_0 + a_0d_1 = 2d_1 + (G''d_0 + G'd_1)x = 2d_1 + \alpha_1x$, $d_0 = \varepsilon_{\perp} - G''(\varkappa + \sigma_H)\cos\theta$, $e_1 = a_0d_0 - a_1d_1 = 2d_0 + (G'd_0 - G''d_1)x = 2d_0 + \alpha_2x$, $d_1 = \sigma_{\perp} + G''(\varkappa + \sigma_H)\cos\theta$,

$x = k_x/k_0$ and $y = k_y/k_0$ are nondimensional wave parameters.

Taking into consideration the boundary condition $\psi(k_x, k_y, L=0) = 0$, from equation (7) for the phase fluctuations we obtain equation (8):

$$\psi(k_x, k_y, L) = \frac{k_0}{4} \int_0^L dz' (e_0 + ie_1)n_1(k_x, k_y, z') \exp \left[-\frac{1}{4}(C_0 + iC_1)k_0(L - z') \right] \quad (8)$$

MCF of the phase fluctuation of a radio signal received on the ground containing useful information about ionospheric irregularities is as equation (9):

$$W_{\varphi}(\eta_x, \eta_y, L) = \pi k_0^4 L \int_{-\infty}^{\infty} dx \int_{-\infty}^{\infty} dy (e_0^2 + e_1^2) V_n(k_0x, k_0y, k_0\Lambda_0) \exp(-i\eta_x x - i\eta_y y) \quad (9)$$

here: $\Lambda_0 = (h_0x^2 + h_1x + h_2)/4$, $h_0 = (G'^2 + G''^2) + (G''P'' - G'P')(y + \mu)$, $h_2 = 2(y^2 + 2\mu y)$, $h_1 = G'y^2 + 2(G'\mu - P')y + 2(G' - P'\mu)$, L is a distance propagating by the radio wave in the ionosphere, $V_n(k_x, k_y, k_z)$ is the arbitrary correlation function of electron density fluctuations, η_x and η_y are small distances between observation points in the XOY plane.

Small-scale plasmonic structures (from hundreds of meters up to kilometers) mainly influence on the amplitude scintillation of radio signals, while the large-scale irregularities give a contribution to the phase fluctuations. The spatial correlation function (9) and the scintillation index S_4 describing an expected diffraction pattern on the ground are connected with the phase auto-correlation function (see equation 10) [23]

$$S_4^2 = 4 \int_{-\infty}^{\infty} dx \int_{-\infty}^{\infty} dy W_{\varphi}(x, y) \sin^2[\Upsilon(x^2 + y^2)] \quad (10)$$

here: $\Upsilon = 2k_0^2/k_f^2$, $k_f = \sqrt{4\pi/\lambda z}$ is the Fresnel wavenumber, λ is the signal wavelength, z is a mean distance between the observer and the irregularities.

From this function it is possible to derive the experimental parameters of the scintillation phenomenon in the reception plane.

3. Results

Numerical analyses are performed on an incident RW with a frequency of 40 MHz ($\lambda = 7.5\text{m}$). Plasma parameters at an altitude of 300 km: $u = 0.0012$, $v = 0.0133$; the Fresnel radius and the Fresnel wavenumber are 1.5 km and 2.4 km^{-1} .

The occurrence of 3-m plume-like, wedge structures and VHF/GHz scintillations were observed in F region of the equatorial ionosphere. The height-integrated rms electron density deviation of $\sim 200\text{-m}$ scale irregularities causing 1.7-GHz scintillations maximizes are established in extended 3 -m plume structures^[24]. SFT with the GNSS Earth Observation Network of Japan (GEONET) is sensitive to small-scale plasmonic structures with horizontal linear scales of $\sim 15\text{--}90\text{ km}$. In the equatorial ionosphere the small-scale electron density inhomogeneities range from a few meters to several tens of kilometers^[14].

Measurements of satellite's signal parameters show that moving irregularities in *F*-region of the equatorial ionosphere have a power-law spectrum with a spectral index p . It is associated with the irregularity power spectrum and can be determined from the power spectra of weak scintillations^[23]. The spectral index p mainly varies in the interval 0.5 and 2.5. Magnetic field measurements by the high-resolution Challenging Minisatellite Payload (CHAMP) show^[19,25] that the spectral indices were between 1.4 and 2.6. A range of $p = 2.0 \div 2.2$ was obtained by the Stretched Rohini Satellite Series (SROSSC2). Equatorial phase scintillations have been used to obtain information about the power spectrum of electron density irregularities, which give rise to the scintillations.

Scintillation normally occurs when the Fresnel dimension of the propagating radio wave is of the order of irregularity scales in the ionosphere^[12]. Scintillation activities were classified^[26] into weak $0.17 \leq S_4 \leq 0.3$, moderate $0.3 \leq S_4 \leq 0.5$ and strong $S_4 > 0.5$. Within the weak scatter assumption, only observed $S_4 > 0.3$ index values were used; $S_4 > 0.3$ up to 0.45

was recorded by the GPS satellites. At very weak scintillations $S_4 < 0.2$. At low latitudes, the scintillation easily reaches the strong regime ($S_4 > 0.7$)^[26,27].

We use a "hybrid" spectral function of electron density irregularities containing both anisotropic Gaussian and power-law spectra^[6]

$$V_n(\mathbf{k}) = \frac{A_p \sigma_n^2}{\left[1 + l_{\perp}^2 (k_x^2 + k_y^2) + l_{\parallel}^2 k_z^2\right]^{p/2}} \frac{l_{\parallel}^3}{\chi^2} \exp \left(-\frac{k_x^2 l_{\parallel}^2}{4 \chi^2} - p_1 \frac{k_y^2 l_{\parallel}^2}{4} - p_2 \frac{k_z^2 l_{\parallel}^2}{4} - p_3 k_y k_z l_{\parallel}^2 \right) \quad (11)$$

where: $p_1 = (\sin^2 \gamma_0 + \chi^2 \cos^2 \gamma_0)^{-1} \left[1 + (\chi^2 - 1)^2 \sin^2 \gamma_0 \cos^2 \gamma_0 / \chi^2\right]$, $p_2 = (\sin^2 \gamma_0 + \chi^2 \cos^2 \gamma_0) / \chi^2$, $p_3 = (\chi^2 - 1) \sin \gamma_0 \cos \gamma_0 / 2 \chi^2$; $A_p = \Gamma(p/2) \Gamma[(5 - p)/2] \sin[(p-3)\pi/2]$, $\Gamma(x)$ is the gamma function. The anisotropy factor $\chi = l_{\parallel} / l_{\perp}$ is the axial ratio of the longitudinal and transverse characteristic linear scales of stretched ionospheric irregularities, γ_0 is the inclination angle of extended ionospheric irregularities with respect to the geomagnetic field, σ_n^2 is the variance of electron density turbulence. Anisotropy shape of the ionospheric plasmonic structures is a result of the diffusion processes in the field aligned and field perpendicular directions.

Substituting equation (11) into equation (9) we obtain equation (12)

$$W_{\varphi}(\eta_x, \eta_y, L) = \frac{\pi^{3/2}}{2} \sigma_n^2 \frac{\xi^3 k_0 L}{\chi^2} \int_{-\infty}^{\infty} dx \int_{-\infty}^{\infty} dy \frac{e_0^2 + e_1^2}{(B_0 + B_1)^2} \cdot \exp \left[-\frac{\xi^2}{4} (D_0 x^4 + D_1 x^3 + D_2 x^2 + D_3 x + D_4) \right] \exp(-i \eta_x x - i \eta_y y) \quad (12)$$

here: $e_0 = 2d_1 + (G'' d_0 + G' d_1) x$, $e_1 = 2d_0 + (G' d_0 - G'' d_1) x$, $B_0 = 1 + \frac{\xi^2}{\chi^2} y^2 + \frac{\xi^2}{16} h_2^2$, $\xi = k_0 l_{\parallel}$,

$$B_1 = \xi^2 \left\{ \frac{1}{16} (h_0^2 x^4 + 2h_0 h_1 x^3) + \left[\frac{1}{\chi^2} + \frac{1}{16} (h_1^2 + 2h_0 h_2) \right] x^2 + \frac{\xi^2}{8} h_1 h_2 x \right\}, D_0 = \frac{P_2}{16} h_0^2, D_1 = \frac{P_2}{8} h_0 h_1, D_2 = \frac{1}{\chi^2} + \frac{P_2}{16} h_1^2 + \frac{P_2}{8} h_0 h_2 + p_3 y h_0, D_3 = \frac{P_2}{8} h_1 h_2 + p_3 y h_1, D_4 = p_1 y^2 + \frac{P_2}{16} h_2^2 + p_3 y h_2.$$

The variance of the phase fluctuations at $\eta_x = \eta_y = 0$ can be written as

$$\langle \phi_1^2 \rangle = \frac{\pi^{3/2}}{2} \sigma_n^2 \frac{\xi^3 k_0 L}{\chi^2} \int_{-\infty}^{\infty} dx \int_{-\infty}^{\infty} dy (A_1 + i A_2) V_n [k_0 x, k_0 y, -k_0 (\Phi_2 + i \Phi_1)] \quad (13)$$

where: $A_1 = 4(d_0^2 + d_1^2) - (\alpha_1^2 + \alpha_2^2)x^2$, $A_2 = 2(4d_0 d_1 - \alpha_1 \alpha_2 x^2)$, $\Phi_1 = \frac{1}{4}(g_1 x^2 - g_2 x)$, $\Phi_2 = \frac{1}{4}(g_3 x^2 + g_4 x + g_5)$, $g_1 = (P'G'' + P''G')$, $g_2 = G''y^2 - 2(G'' + P''\mu)$, $g_3 = (G''P'' - G'P')$, $g_4 = G'y^2 + 2(G' - P'\mu)$, $g_5 = 4\mu$.

Substituting equation (12) into equation (13) we obtain equation (14):

$$\langle \phi_1^2 \rangle = \frac{\pi^{3/2}}{2} \sigma_n^2 \frac{\xi^3 k_0 L}{\chi^2} \int_{-\infty}^{\infty} dx \int_{-\infty}^{\infty} dy \frac{1}{\Lambda_3^2 + \Lambda_4^2} [(A_1 \Lambda_3 + A_2 \Lambda_4) + i(A_2 \Lambda_3 - A_1 \Lambda_4)] \cdot \exp\left(-\frac{\xi^2}{4} J_0 + i \frac{\xi^2}{4} J_1\right) \quad (14)$$

where: $\Lambda_1 = g_1 g_3 x^4 + (g_1 g_4 - g_2 g_3)x^3 + (g_1 g_5 - g_2 g_4)x^2 - g_2 g_5 x$, $\Lambda_2 = 1 + \frac{\xi^2}{\chi^2} y^2 + \frac{\xi^2}{16} [(g_3^2 - g_1^2)x^4 + 2(g_1 g_2 + g_3 g_4)x^3 + (g_4^2 - g_2^2 + 2g_3 g_5 + \frac{16}{\chi^2})x^2 + 2g_4 g_5 x + g_5^2]$, $\Lambda_3 = \Lambda_2^2 - \frac{\xi^4}{64} \Lambda_1^2$, $\Lambda_4 = \frac{\xi^2}{4} \Lambda_1 \Lambda_2$, $J_1 = \frac{P_2}{8} \Lambda_1 - 4p_3 y \Phi_1$, $J_0 = p_1 y^2 - 4p_3 y \Phi_2 + \frac{P_2}{16} [(g_3^2 - g_1^2)x^4 + 2(g_1 g_2 + g_3 g_4)x^3 + (g_4^2 - g_2^2 + 2g_3 g_5 + \frac{16}{\chi^2})x^2 + 2g_4 g_5 x + g_5^2]$.

Figure 1 represents deviation of the O- and E-waves ray paths for two layered irregular slabs in the equatorial ionosphere. This figure illustrates the equatorial anomaly characterizing the low-latitude terrestrial ionosphere. Such an anomaly is the ‘‘Foun-

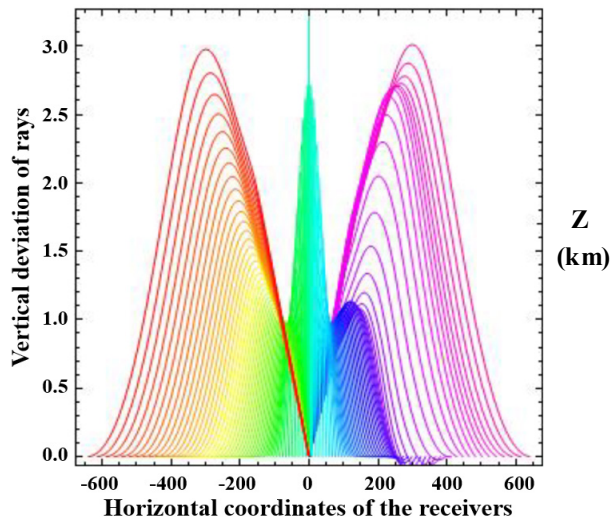


Figure 1. Deviation of the O- and E-waves ray paths for two layered irregular slabs in the equatorial ionosphere.

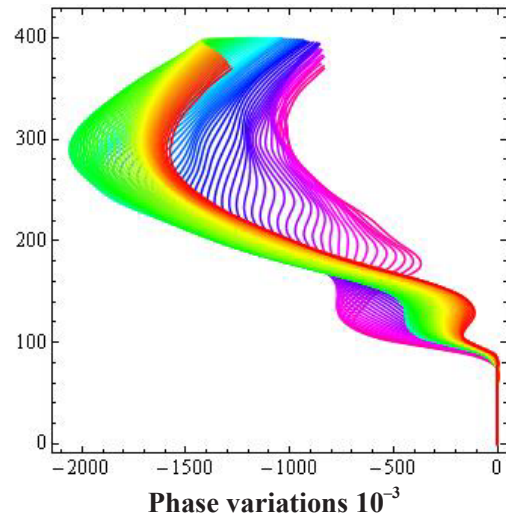


Figure 2. The dependence of the phase variations between the O- and E-waves versus altitude in a low-latitude ionosphere.

tain Effect” of the deviation of O- and E- waves from the straight line connecting the source and receiver. Spacecrafts moving at a distance of 400 km from the Earth surface. The frequency of a radiating RW is 430 MHz. The receiver is located on a surface. The plasma rises upward in the equatorial region and gradually turns north in the northern hemisphere and south in the southern, which is caused by an increase in the inclination of geomagnetic lines of force on both sides of the geomagnetic equator. Two crests arise on both sides of the geomagnetic equator corresponding to O- and E- waves. At latitudes adjacent to the geomagnetic equator, there are stratification of large-scale irregularities in the F2 region of the ionosphere new additional layers appear. An additional extremum in the center of the figure arises due to the central perturbation, with the central extremum having different signs depending on the sign of the central inhomogeneity. This equatorial anomaly is an important factor in predicting the parameters of radio communication, radio navigation, location, signifi-

cantly affects the operation of various ground-based technological systems, etc.

Figure 2 represents the dependence of the phase variations between the O- and E-waves versus altitude in a low-latitude ionosphere. This figure illustrates phase variations as a function of the altitude. Minimums of the curves correspond to the maximums of the ionospheric layers; local maximums correspond to the interlayer valleys. Deep minimum in height corresponds to the maximum of the electron density in the equatorial anomaly; minimums and maximums at the bottom of the figure correspond to the rays crossing the ionospheric layer at different angles.

Figure 3 illustrates the scintillation level as a function of the RMS deviation of the phase fluctuations of scattered radio waves in the equatorial ionosphere. Power-law spectral index p of the phase correlation function (3.1) is associated with the scintillation index. Numerical calculations are performed using the data from experimental observations^[26] at $p = 0.5 \div 2.5$.

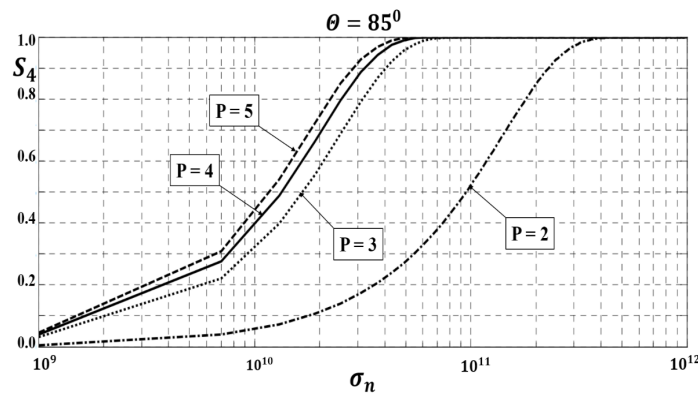


Figure 3. The dependence of the scintillation index S_4 on the variance of the normalized RSD of electron density fluctuations σ_n at different phase spectral index p and the slope (apex) angle of the satellite radio navigation system $\Theta = 85^\circ$.

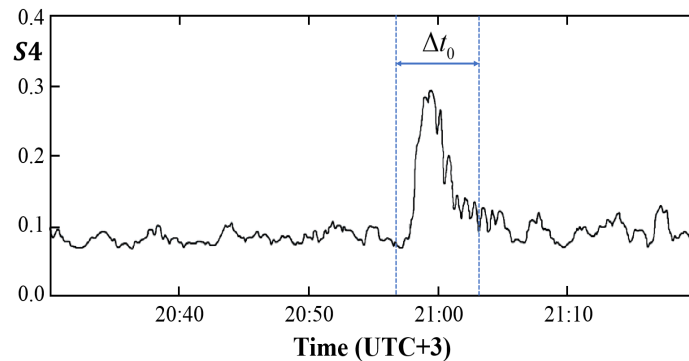


Figure 4. Monitoring of the scintillation index S_4 at different observation time intervals.

Figure 4 illustrates mainly weak temporal variations of the scintillation index $S_4 = 0.7 \div 0.3$ at different observation time intervals. Scintillation level reaches its maximum value at night: 21:00 hour, then gradually decreases. Frequency of the navigation satellite PRN2 GPS SRNS signal is about 1 GHz.

Figure 5 illustrates moderate variations of the scintillation index when the GPS crosses the region with small-scale electron density irregularities. The weak scintillation is observed $S_4 \approx 0.15$ mainly at the same time intervals, sometimes scintillation becomes moderate $S_4 \approx 0.35$ during $\Delta t \approx 40$ min. In this case, the GPS cross the region in the equatorial ionosphere with small-scale electron density inhomogeneities.

Figure 6 illustrates the dependence of the weak scintillation index S_4 versus anisotropy parameter χ of extended irregularities for different slop angle γ_0 at weak and moderate scintillations in the equatorial ionosphere. Black curves correspond to the O-wave, vi-

olet curves are devoted to the E-waves. Curves 1 and 4 are related to the inclinations angle $\gamma_0 = 0^\circ$, curves 2 and 5—to the tilt angle $\gamma_0 = 10^\circ$ and curves 3 and 6—to the tilt angle $\gamma_0 = 30^\circ$. Maximum of S_4 curves are devoted to the O- wave is shifted to the right $\chi = 15.66 \div 16.4$; maximum relating to the E-wave is displaced to the left in the interval $\chi = 18.7 \div 18.5$.

4. Discussion

This paper examines the influence of ionospheric scintillations caused by RSD of the electron density fluctuation in the equatorial ionosphere on the fluctuation of the phase of the navigation radio signal analytically calculating polarization coefficients and second order statistical moments of scattered RWs for the first time. Analytical investigations are performed using the Wentzel-Kramers-Brillouin method for small-scale electron density irregularities. Correlation function of the phase fluctuations has

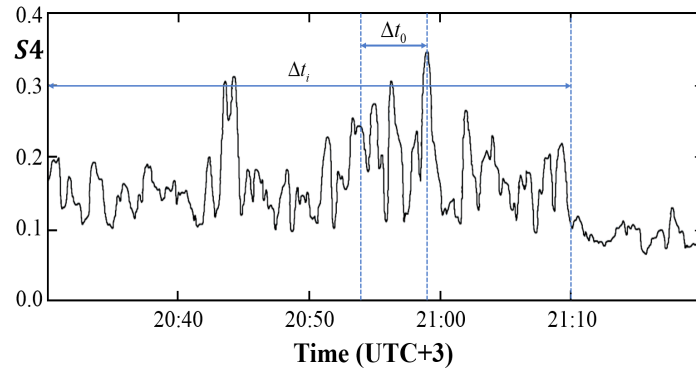


Figure 5. Moderate scintillation of navigation radio signals of the GPS system at night in the equatorial terrestrial ionosphere.

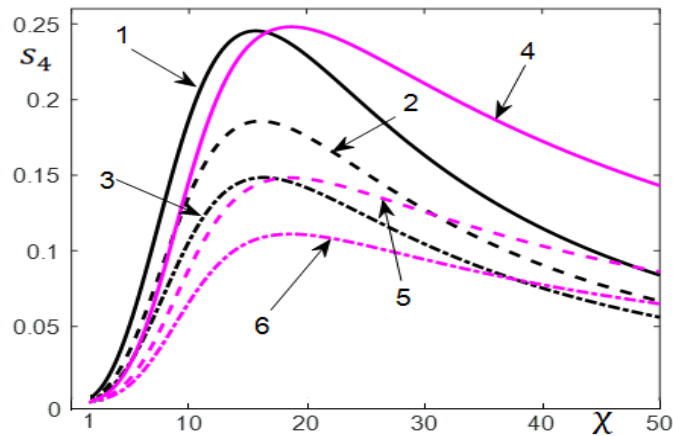


Figure 6. Scintillation index versus anisotropy coefficient of prolate electron density inhomogeneities.

been obtained for arbitrary MCF of electron density fluctuations containing complex permittivity and conductivities (Hall, Pedersen and longitudinal) of the equatorial ionosphere for both O- and E-waves and also anisotropy parameters characterizing elongated electron density irregularities. New peculiarities of the “Fontan Effect” have been revealed in the equatorial using the experimental observations of the GNSS radiating radio signals at the frequency of 1 GHz. The crests occur at the geomagnetic equator corresponding to the O- and E- waves. A spectral index of the “hybrid” power-law spectrum of electron density fluctuations has been applied using the experimental data. GPS observation data has been analyzed. It was shown that weak and moderate scintillations arise in the equatorial ionosphere propagating radio signals through the small-scale electron density irregularities. A new feature of the “Fountain Effect” has been discovered in the equatorial ionosphere at weak and moderate scintillations caused due to anisotropy parameters of electron density fluctuations. The slope angle of elongated plasmonic irregularities shifts the maximum of the O- and E- waves in opposite directions.

Investigation of the scintillation effects and ionospheric irregularities is an actual problem for RWs propagation in the terrestrial ionosphere, plasma turbulence, development and application of the observation systems.

The obtained results are very encouraging. Indeed, one of the deficiencies of scintillation theory is the vague link between the observable scintillation parameters and the physics of the processes that are responsible for producing the irregularities in the conductive polar ionosphere. The general morphology of ionospheric scintillation is reasonably well known. The results presented in this paper suggest that a careful study of the scintillation statistics might reveal some new insight into the mechanisms that are involved. The obtained results will have wide applications in both natural and laboratory plasmas.

Author Contributions

Conceptualization, G.J.; Methodology, G.J.; Soft-

ware Z.S., N.M.; Investigation, G.J.; Data curation, G.J.; Writing -Original draft, G.J.; Visualisation, Z.S., N.M. All authors have read and agreed to the published version of the manuscript.

Conflict of Interest

There is no conflict of interest.

Funding

This work was supported by Shota Rustaveli National Science Foundation of Georgia (SRNSFG), grant NFR-21-316 “Investigation of the statistical characteristics of scattered electromagnetic waves in the terrestrial atmosphere and application”.

References

- [1] Gershman, B.N., Erukhimov, L.M., Yashin, Y.Y., 1984. Wave phenomena in the Ionosphere and Space Plasma. Moscow, Nauka. Available from: <https://www.scirp.org/reference/referencespapers?referenceid=479241>(in Russian)
- [2] Ishimaru, A., 1997. Wave propagation and scattering in random media, vol. 2: multiple scattering, turbulence, rough surfaces and remote sensing. IEEE Press: Piscataway, New Jersey, USA.
- [3] Basu, S., Basu, S., 1981. Equatorial scintillations—a review. Journal of Atmospheric and Terrestrial Physics. 43(5–6), 473–489.
- [4] Maruyama, T., Matuura, N., 1984. Longitudinal variability of annual changes in activity of equatorial spread *F* and plasma bubbles. Journal of Geophysical Research. 89(12), 10903–10912.
DOI: <https://doi.org/10.1029/JA089iA12p10903>
- [5] Yeh, K. C., Liu, C-H., 1982. Radio wave scintillations in the ionosphere. IEEE Proceedings. 70, 324–360.
- [6] Kintner P. M, Ledvina B. M, de Paula E. R., 2007. GPS and ionospheric scintillations. Space Weather. 5(9).
- [7] Jandieri, G., Ishimaru, A., Rawat, B., et al.,

2017. Statistical moments and scintillation level of scattered electromagnetic waves in the magnetized plasma. *Advanced Electromagnetics*. 7(3).
- [8] Jandieri, G, Ishimaru, A, Rawat, B, et al., 2017. Power spectra of ionospheric scintillations. *Advanced Electromagnetics*. 6(4).
- [9] Jandieri, G., Ishimaru, A., Gavrilenko, V.G., et al., 2023. Power spectra of radio waves scintillation in the high-latitude conductive terrestrial ionosphere. *Bulletin of TICMI*. 27(2), 81–94.
- [10] Jandieri, G., Tugushi, N., 2023. Statistical characteristics of the temporal spectrum of scattered radiation in the equatorial ionosphere. *Journal of Environmental and Earth Sciences*. 5(1) 85–94.
- [11] Jandieri, G., Tugushi, N., 2023. Transformation of the spatial spectrum of scattered radio waves in the conductive equatorial ionosphere. *Electronics*. 12(13), 2759.
- [12] Sharon, A., Stephan, B., Jurua, E., 2020. Ionospheric irregularities and scintillations: a direct comparison of in situ density observations with ground-based L-band receivers. *Earth, Planets and Space*. 72(164), 1–15.
- [13] Woodman, R. F, La Hoz, C., 1976. Radar observations of F region equatorial irregularities. *Journal of Geophysical Research*. 81(31), 5447–5466.
- [14] McClure, J. P, Hanson, W. B, Hoffman, J. H., 1977. Plasma bubbles and irregularities in the equatorial ionosphere. *Journal of Geophysical Research (Space Physics)*. 82(19), 2650–2656,
- [15] Burke, W. J, Huang, C. Y, Valladares, C. E, et al., 2003. Multipoint observations of equatorial plasma bubbles, *Journal of Geophysical Research (Space Physics)*. 108(A5), 1221.
- [16] Sarkar, S, Gwal, A., 2014. Coordinated in situ measurements of plasma irregularities and ground based scintillation observations at the crest of equatorial anomaly. *Advances in Space Research*. 54(3), 425–434.
- [17] Ott, E., 1978. Theory of rayleigh-taylor bubbles in the equatorial ionosphere. *Journal of Geophysical Research*. 83(A5), 2066–2070.
- [18] Vankadara, R.K., Jamjareegulgarn, P., Seemala, G.K., et al., 2023. Trailing equatorial plasma bubble occurrences at a low-latitude location through Multi-GNSS slant TEC depletions during the strong geomagnetic storms in the ascending phase of the 25th solar cycle. *Remote sensing*. 15(20), 4944.
- [19] Ma, G., Li, Q., Li, J., et al., 2020. Study of ionospheric irregularities with spatial fluctuation of TEC. *Journal of Atmospheric and Solar-Terrestrial Physics*. 211, 105485.
- [20] Huang, C-S., La Beaujardiere, O., Roddy, P., et al., 2014. Occurrence probability and amplitude of equatorial ionospheric irregularities associated with plasma bubbles during low and moderate solar activities (2008–2012). *Journal of Geophysical Research: Space Physics*. 119(2), 1186–1199.
- [21] Huang, F., Lei, J., Xiong, C., et al., 2021. Observations of equatorial plasma bubbles during the geomagnetic storm of October 2016. *Earth Planetary Physics*. 5(5),416–426.
- [22] Aydogdu, M., Guzel, E., Yesil, A., et al., 2007. Comparison of the calculated absorption and the measured field strength of HF waves reflected from the ionosphere. *Nuovo Cimento-Societa Italiana di Fisica Sezione C*. 30(3), 243–253.
- [23] Rufenach, C.L., 1972. Power-law wave number spectrum deduced from ionospheric scintillation observations. *Journal of Geophysical Research*. 77(25), 4761–4772.
- [24] Basu, S., Basu, S., LaBelle, J., et al., 1986. Gigahertz scintillations and spaced receiver drift measurements during project Condor Equatorial F-region rocket campaign in Peru. *Journal of Geophysical Research: Space Physics*. 91(A5), 5526–5538.
- [25] Patel, K., Singh A.K., Subrahmanyam, P., et al., 2011. Modeling of ionospheric scintillation at low-latitude. *Advances in Space Research*. 47(3), 515–524.
- [26] Yang, Z., Morton, Y.T.J., 2020. Low-latitude

GNSS ionospheric scintillation dependence on magnetic field orientation and impacts on positioning. *Journal of Geodesy*. 94(59).

DOI: <https://doi.org/10.1007/s00190-020-01391-7>

[27] Alfonsi, L., Wernik, A.W., Materassi, M., et al., 2017. Modelling ionospheric scintillation under the crest of the equatorial anomaly. *Advances in Space Research*. 60(8), 1698–1707.